

# First demonstration of rainbow photocatalysts using ternary $\text{Cd}_{1-x}\text{Zn}_x\text{Se}$ nanorods of varying compositions

An T. Nguyen, Wei-Hao Lin, Yi-Hsuan Lu, Yao-De Chiou, Yung-Jung Hsu\*

Department of Materials Science and Engineering, National Chiao Tung University, Hsinchu, Taiwan 30010, Republic of China

## ARTICLE INFO

### Article history:

Received 30 October 2013

Received in revised form 21 January 2014

Accepted 13 February 2014

Available online 20 February 2014

### Keywords:

Rainbow photocatalysts

Solar fuel production

$\text{Cd}_{1-x}\text{Zn}_x\text{Se}$

Cation exchange

## ABSTRACT

We demonstrated for the first time that the assembly of  $\text{Cd}_{1-x}\text{Zn}_x\text{Se}$  nanorods (NRs) with five compositions ( $x = 0, 0.35, 0.54, 0.61, 1$ ) may absorb the whole visible spectrum in a gradient fashion for photoconversion applications. The samples were prepared by conducting cation exchange reactions on  $\text{Ag}_2\text{Se}$  NRs with excess  $\text{Cd}^{2+}$  and  $\text{Zn}^{2+}$  ions. By modulating the molar ratio of  $\text{Cd}^{2+}$  to  $\text{Zn}^{2+}$  employed, the composition of the resulting  $\text{Cd}_{1-x}\text{Zn}_x\text{Se}$  NRs can be delicately controlled. Because of the tunability of band edge with stoichiometry,  $\text{Cd}_{1-x}\text{Zn}_x\text{Se}$  NRs of varying compositions absorbed light at different wavelength regions, which spanned almost the entire visible spectrum. As compared to the individual constituent NRs, the NRs assembly exhibited greatly improved photoactivity in photoelectrochemical water splitting as well as superior photocatalytic performance toward methylene blue degradation under white light illumination. This superiority emanates from the composition-gradient configuration that significantly improves the light harvesting efficiency by absorbing almost the whole visible spectrum of the incident white light. The full visible photon harvesting of the NRs assembly was validated by the photocurrent action spectrum which showed spectral accordance with the absorption spectrum. The recycling test manifests that the NRs assembly displayed substantially high stability during its use as photocatalyst. Furthermore, the result of performance evaluation under natural sunlight reveals that the present NRs assembly can be used as practical rainbow photocatalysts which may effectively harvest energy from sunlight. The demonstration from this work may facilitate the use of sophisticated assembly of semiconductor nanocrystals in relevant photoconversion processes where the effectiveness of photon harvesting is determinant.

© 2014 Elsevier B.V. All rights reserved.

## 1. Introduction

Ternary chalcogenide nanocrystals such as  $\text{Cd}_{1-x}\text{Zn}_x\text{S}$  [1–3],  $\text{Cd}_{1-x}\text{Zn}_x\text{Se}$  [4–6], and  $\text{CdS}_{1-x}\text{Se}_x$  [7–9] have received considerable attention because their composition-tunable band edge offers new opportunities to harvest light energy in the entire visible region of solar spectrum. Of particular importance is the development of tandem solar cells in which an assembly of ternary alloyed nanocrystals with different compositions is employed to harvest photons in a gradient fashion [10]. Systematic combination of these nanocrystals constituting gradient alloyed structures can provide synergy for capturing and converting a wide array of photons in the visible region, which conduces to effective carrier utilization and therefore improves the photoconversion efficiency. Such extendable light harvesting feature for ternary chalcogenide nanocrystals opens up a multitude of potential applications in a

wide array of fields, which include photovoltaics [11–13], photocatalysis [14–17], and photoelectrochemical cells [18–20]. The possibility of enhancing light harvesting is especially important to photocatalytic solar fuel production. For photocatalysis operation, it is desirable that light absorption of photocatalysts could span large region of solar spectrum to enable full photon harvesting. However, even when photons are completely absorbed, photon energy that exceeds semiconductor bandgap is dissipated as heat due to the vibrational relaxation of excitons [21,22]. Because of the heat loss, a substantial amount of solar energy has already been consumed before it can be converted into other accessible energies. This obstacle needs to be circumvented to promote the advancement of photocatalysis technology for solar fuel production.

Cation exchange reaction has been demonstrated as a simple yet efficient synthetic approach for preparation of ionic nanocrystals [23,24]. One key aspect of this reaction is that the anionic framework is maintained throughout the ion diffusion process, yielding nanocrystals that preserve the morphology and crystallinity of the starting materials. Since the pioneering work by Alivisatos and co-workers [25], cation exchange reaction has been widely

\* Corresponding author. Tel.: +886 3 5712121x55317; fax: +886 3 5724724.  
E-mail addresses: [yhsu@cc.nctu.edu.tw](mailto:yhsu@cc.nctu.edu.tw), [yhsu@mail.nctu.edu.tw](mailto:yhsu@mail.nctu.edu.tw) (Y.-J. Hsu).

employed to prepare chalcogenide semiconductor nanocrystals, especially those with structural and compositional diversities. Through carefully controlling the reaction conditions of cation exchange, various types of semiconductor nanoheterostructures including alloy nanocrystals [26–28], doped nanocrystals [29,30], core-shell structures [31–35], and segmented structures [36–40] can be readily obtained. These demonstrations address the feasibility of cation exchange in fabrication of nanostructures that are difficult to be prepared with the general methods.

In this work, we demonstrated that the assembly of  $\text{Cd}_{1-x}\text{Zn}_x\text{Se}$  nanorods (NRs) with five different compositions ( $x=0, 0.35, 0.54, 0.61, 1$ ) may absorb the whole visible spectrum for photoconversion applications, in which Zn-rich NRs harvested high-energy photons whereas low-energy photons were mainly captured by Cd-rich NRs. This is the first demonstration for rainbow photocatalysts which absorb solar energy in a gradient fashion by using  $\text{Cd}_{1-x}\text{Zn}_x\text{Se}$  NRs of varying compositions. The samples were prepared by conducting cation exchange reaction on  $\text{Ag}_2\text{Se}$  NRs with excess  $\text{Cd}^{2+}$  and  $\text{Zn}^{2+}$  ions in the presence of tributylphosphine at 65 °C. By modulating the molar ratio of  $\text{Cd}^{2+}$  to  $\text{Zn}^{2+}$  employed, the composition of the resulting  $\text{Cd}_{1-x}\text{Zn}_x\text{Se}$  NRs can be delicately controlled. By virtue of the structural preservation feature of cation exchange reaction, the five  $\text{Cd}_{1-x}\text{Zn}_x\text{Se}$  NR products possessed fairly similar dimensions, which is difficult to be achieved using other synthetic approaches. This feature is especially important to the interpretation of the resultant photocatalytic performance since the possible size variation effect could be excluded. Because of the tunability of band edge with stoichiometry,  $\text{Cd}_{1-x}\text{Zn}_x\text{Se}$  NRs of varying compositions absorbed light at different wavelength regions, which spanned almost the entire visible spectrum. Unlike most studies concerning the photocatalytic performance of  $\text{Cd}_{1-x}\text{Zn}_x\text{Se}$  which explored the effect of  $\text{Cd}^{2+}$  to  $\text{Zn}^{2+}$  ratio, the current study focuses on studying the influence of composition assembly on the overall photoconversion efficiency of the samples. As compared to the individual constituent NRs, the NRs assembly exhibited higher photocurrents of water splitting as well as superior photocatalytic performance under white light illumination, attributable to the broadband light absorption feature that enables full visible photon harvesting. Besides, no appreciable decay of photocatalytic activity was found for the NRs assembly after repeatedly used and recycled in dye photodegradation for four times, manifesting its substantially high stability during the course of photocatalysis. Furthermore, the photocatalytic performance under natural sunlight was also tested, and the result shows that the present NRs assembly can be used as practical rainbow photocatalysts for efficient solar fuel production.

## 2. Experimental

### 2.1. Chemicals

All chemicals were of analytical grade and used without further purification. Special attention should be paid when dealing with the hazardous Cd source.

### 2.2. Preparation of Se NRs

Se NRs were prepared using a chemical reduction method developed by our group [41]. Briefly,  $\text{SeO}_2$  powder (1.0 mmol) was dissolved in an aqueous solution of carboxymethyl cellulose (denoted as CMC, Mw = 90000 Da, 9.0 mL, 4.0 wt%), followed by the addition of NaOH solution (1.0 mL, 1.0 M) under vigorous stirring at room temperature. When the mixed solution became transparent,  $\text{NaBH}_4$  solution (1.0 mL, 1.0 M) was added to carry out the reduction reaction. After stirring at 25 °C for 2 h, brown suspending solids

(Se NRs) were produced. The samples were collected, washed, and dried at 60 °C in vacuum for later use.

### 2.3. Transformation of Se NRs into $\text{Ag}_2\text{Se}$ NRs

A given amount of Se NRs (0.5 mmol) were re-dispersed in deionized water (10 mL) to serve as the growth template for  $\text{Ag}_2\text{Se}$ . The growth of  $\text{Ag}_2\text{Se}$  NRs was performed by gradually injecting  $\text{AgNO}_3$  solution (1.25 mmol, 5 mL) into the Se NRs suspension under vigorous stirring at 25 °C. The transformation finished in 2 h as the color of the reaction solution became black. The product ( $\text{Ag}_2\text{Se}$  NRs) was collected, washed, and dried at 60 °C in vacuum for later use.

### 2.4. Cation exchange reaction for $\text{Cd}_{1-x}\text{Zn}_x\text{Se}$ NRs growth

A given amount of  $\text{Ag}_2\text{Se}$  NRs (0.05 mmol) were re-dispersed in methanol (10 mL) for use as the reactant in cation exchange reaction. In a typical procedure,  $\text{Cd}(\text{NO}_3)_2$  and  $\text{Zn}(\text{NO}_3)_2$  with a desired molar ratio (total amount = 1.0 mmol) were dissolved in methanol solution (40 mL) containing poly(N-vinylpyrrolidone) (denoted as PVP, Mw = 10,000 Da, 0.5 g). The premixed solution of  $\text{Cd}^{2+}$  and  $\text{Zn}^{2+}$  was then added to the  $\text{Ag}_2\text{Se}$  NRs suspension, after which 0.2 mL of tributylphosphine (denoted as TBP) was injected at 65 °C to proceed with cation exchange reaction. The cation exchange completed in 2 h as the color of reaction solution turned to brownish-yellow. The product ( $\text{Cd}_{1-x}\text{Zn}_x\text{Se}$  NRs) was collected, washed, and dried at 60 °C in vacuum for later characterizations. In this work, various molar ratios of  $\text{Cd}^{2+}$  to  $\text{Zn}^{2+}$  (1:0, 1:1, 1:2, 1:4, 0:1) added in cation exchange reaction were employed to prepare  $\text{Cd}_{1-x}\text{Zn}_x\text{Se}$  NRs of varying compositions. From energy dispersive X-ray spectrometry (EDS) analysis, the composition of the NRs product was determined to be pure  $\text{CdSe}$ ,  $\text{Cd}_{0.65}\text{Zn}_{0.35}\text{Se}$ ,  $\text{Cd}_{0.46}\text{Zn}_{0.54}\text{Se}$ ,  $\text{Cd}_{0.39}\text{Zn}_{0.61}\text{Se}$ , and pure  $\text{ZnSe}$  for the employment of  $\text{Cd}^{2+}/\text{Zn}^{2+}$  ratio of 1:0, 1:1, 1:2, 1:4, and 0:1, respectively.

### 2.5. Photoelectrochemical measurement

The photoelectrochemical measurement was conducted in a three-electrode cell which consisted of Pt counter electrode,  $\text{Ag}/\text{AgCl}$  reference electrode and 0.1 M  $\text{Na}_2\text{S}$  electrolyte.  $\text{Na}_2\text{S}$  was employed as a hole scavenger to prevent the photocorrosion of the samples, which may ensure efficient hydrogen production at the cathode. The photoanode was prepared by dripping sample suspension (20  $\mu\text{L}$ , 1.0 mg/mL) on the fluorine-doped tin oxide (FTO) substrate (1.0 cm × 1.0 cm). After completely dried, the substrate was inserted in the three-electrode cell for measurement. The photoelectrochemical data were collected in an electrochemical station under white light illumination (500 W xenon lamp, with a light intensity of 100 mW/cm<sup>2</sup>). The photocurrent action spectra were measured under illumination of monochromatic light from the xenon lamp coupled with a monochromator.

### 2.6. Photocatalytic performance measurement

The photocatalytic performance of the samples was evaluated by monitoring the photodegradation of methylene blue (denoted as MB) under white light illumination (500 W xenon lamp, with a light intensity of 100 mM/cm<sup>2</sup>). Note that white light irradiation, which matches well natural sunlight in spectral distribution, was applied in order to demonstrate the applicability of the samples in solar fuel production. A quartz tube with a capacity of 30 mL was used as the photoreactor vessel. Six kinds of photocatalysts including pure  $\text{CdSe}$  NRs, pure  $\text{ZnSe}$  NRs, the three individual  $\text{Cd}_{1-x}\text{Zn}_x\text{Se}$  NRs, and the NRs assembly were compared in the photodegradation of MB. The NRs assembly was prepared by mixing equal weights

of pure CdSe, pure ZnSe, and the three  $\text{Cd}_{1-x}\text{Zn}_x\text{Se}$  NRs. A typical experiment involved adding 5.0 mg of photocatalyst to 20 mL of MB aqueous solution ( $1.0 \times 10^{-5}$  M) in the photoreactor vessel. Prior to irradiation, the suspension was aerated and stirred in the dark for 30 min to reach the adsorption equilibrium of MB with photocatalyst. At certain time intervals of irradiation, 1 mL aliquots of reaction solution were withdrawn and centrifuged to remove the photocatalyst particles. The UV-visible absorption spectra of the filtrates were then acquired to measure the concentration variation of MB by recording the corresponding absorbance of the characteristic peak at 665 nm. Furthermore, degradation of MB ( $1.0 \times 10^{-5}$  M) under natural sunlight by using the NRs assembly as photocatalyst was also examined.

### 2.7. Characterizations

The morphology and dimensions of the products were observed with a field-emission scanning electron microscope (FESEM, JEOL, JSM-6500F). The crystallographic structure of the samples was investigated with X-ray diffraction (XRD, MAC Science, MXP18) and high-resolution transmission electron microscopy (HRTEM, JEOL, JEM-3000). The elemental analysis of NRs was conducted with EDS, the accessory of SEM (JSM-6500F) and TEM (JEM-3000). The composition of  $\text{Cd}_{1-x}\text{Zn}_x\text{Se}$  NRs was determined by examining three batches of samples, from which an average value was calculated and represented. UV-visible absorption spectra were obtained using a Hitachi U-3900H spectrophotometer at room temperature. The Brunauer–Emmett–Teller (BET) specific surface areas of the samples were estimated from the  $\text{N}_2$  adsorption–desorption analysis.

## 3. Results and discussion

Single-crystalline Se NRs with trigonal crystallographic structure were first prepared using the CMC-stabilized chemical reduction method [41]. By reacting with  $\text{AgNO}_3$  at room temperature, trigonal Se can be completely transformed into orthorhombic  $\text{Ag}_2\text{Se}$  due to the topotactic lattice matching [23]. As shown in Fig. 1, the thus-obtained  $\text{Ag}_2\text{Se}$  NRs inherited the dimensions of the initial Se, which had a typical diameter of around 100 nm and length up to 1  $\mu\text{m}$ . Further replacement of  $\text{Ag}^+$  of  $\text{Ag}_2\text{Se}$  NRs with  $\text{Cd}^{2+}$  can be achieved by conducting cation exchange reaction in the presence of TBP at an elevated temperature of 65 °C. Note that the conversion from  $\text{Ag}_2\text{Se}$  to CdSe via cation exchange is thermodynamically unfavorable unless a complexation ligand is introduced at the elevated reaction temperature [24]. Specifically, the complexation of

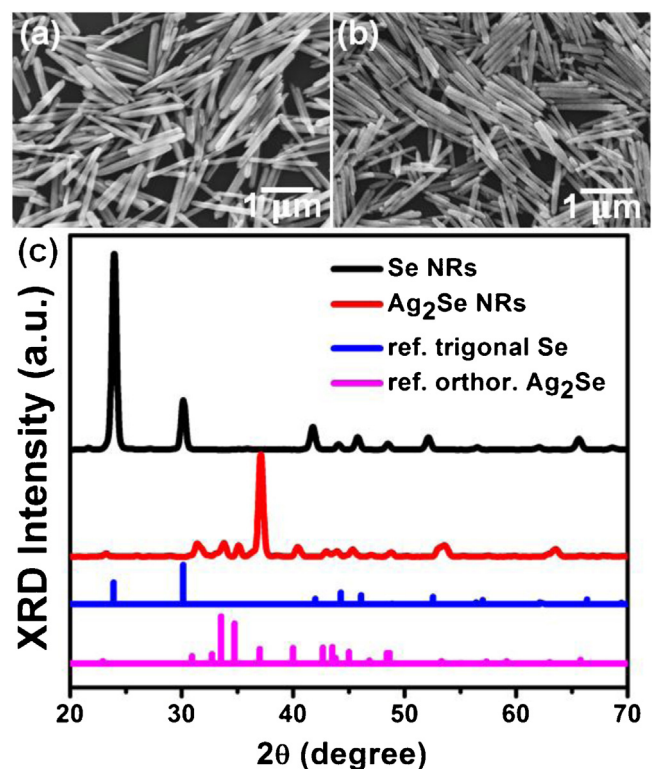


**Fig. 1.** SEM images of (a) Se NRs and (b)  $\text{Ag}_2\text{Se}$  NRs. The corresponding XRD patterns were shown in (c). The patterns of reference trigonal Se (JCPDS 06-0362) and orthorhombic  $\text{Ag}_2\text{Se}$  (JCPDS 24-1041) were also included for comparison.

TBP with  $\text{Ag}^+$  of  $\text{Ag}_2\text{Se}$  may facilitate the replacement of  $\text{Ag}^+$  by  $\text{Cd}^{2+}$  at the anionic framework of NRs, which is conducive to the successful transformation of  $\text{Ag}_2\text{Se}$  into CdSe. The same situation stands for the conversion to ZnSe since ZnSe is more prone to solvation when accompanying  $\text{Ag}_2\text{Se}$  [24]. Besides, the transformation from  $\text{Ag}_2\text{Se}$  into ZnSe took more time to finish, presumably resulting from the relatively lower reactivity of  $\text{Zn}^{2+}$  in the cation exchange reaction. As displayed in Fig. 2, the resulting CdSe and ZnSe also preserved NR morphology that adopted the reactant  $\text{Ag}_2\text{Se}$ . Also presented in Fig. 2 are the SEM images of the samples obtained by adding both  $\text{Cd}^{2+}$  and  $\text{Zn}^{2+}$  in the cation exchange reaction. Interestingly, as  $\text{Cd}^{2+}$  and  $\text{Zn}^{2+}$  were co-fed in the transformation of  $\text{Ag}_2\text{Se}$ , NRs with high structural uniformity were still grown. SEM-EDS analysis shows that the composition of the composite NRs prepared with  $\text{Cd}^{2+}/\text{Zn}^{2+}$

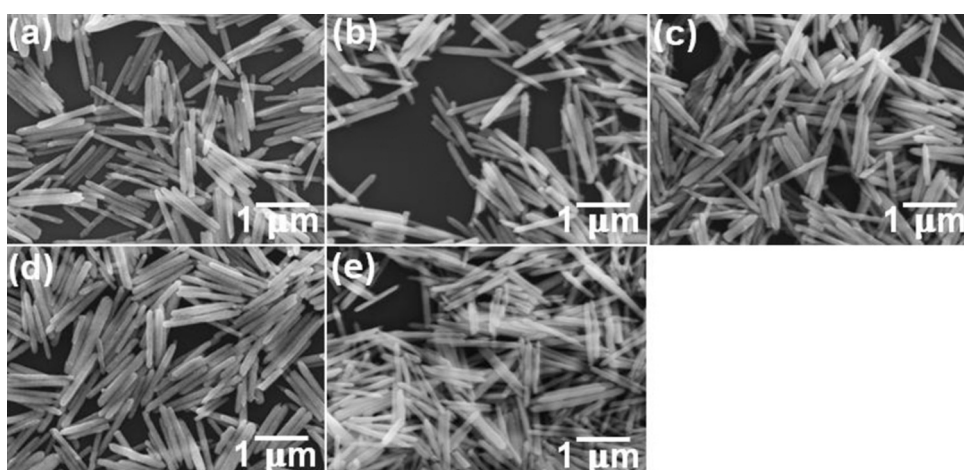


**Fig. 2.** SEM images of (a) pure CdSe, (b)  $\text{Cd}_{0.65}\text{Zn}_{0.35}\text{Se}$ , (c)  $\text{Cd}_{0.46}\text{Zn}_{0.54}\text{Se}$ , (d)  $\text{Cd}_{0.39}\text{Zn}_{0.61}\text{Se}$ , and (e) pure ZnSe NRs derived from  $\text{Ag}_2\text{Se}$  NRs via cation exchange.

ratio of 1:1, 1:2, and 1:4 was  $\text{Cd}_{0.65}\text{Zn}_{0.35}\text{Se}$ ,  $\text{Cd}_{0.46}\text{Zn}_{0.54}\text{Se}$ , and  $\text{Cd}_{0.39}\text{Zn}_{0.61}\text{Se}$ , respectively. This outcome indicates that concurrent exchange for  $\text{Cd}^{2+}$  and  $\text{Zn}^{2+}$  may have occurred at the anionic framework of  $\text{Ag}_2\text{Se}$  to lead to the formation of ternary  $\text{Cd}_{1-x}\text{Zn}_x\text{Se}$ . The average size and size distribution of the NR samples were determined by counting over 25 NRs from the SEM images. The diameter and length were  $105 \pm 8 \text{ nm}$  and  $1092 \pm 88 \text{ nm}$ ,  $108 \pm 12 \text{ nm}$  and  $1095 \pm 70 \text{ nm}$ ,  $105 \pm 7 \text{ nm}$  and  $1094 \pm 81 \text{ nm}$ ,  $109 \pm 11 \text{ nm}$  and  $1098 \pm 59 \text{ nm}$  and  $106 \pm 9 \text{ nm}$  and  $1095 \pm 77 \text{ nm}$  for pure  $\text{CdSe}$ ,  $\text{Cd}_{0.65}\text{Zn}_{0.35}\text{Se}$ ,  $\text{Cd}_{0.46}\text{Zn}_{0.54}\text{Se}$ ,  $\text{Cd}_{0.39}\text{Zn}_{0.61}\text{Se}$  and pure  $\text{ZnSe}$  NRs, respectively.

To identify the chemical composition and crystallographic structure for the samples derived from  $\text{Ag}_2\text{Se}$ , XRD measurement was performed. As Fig. 3 shows, the patterns characterized the three types of NRs as wurtzite II–VI semiconductor compounds. For pure  $\text{CdSe}$  NRs, they were grown as wurtzite structure because of the topotactic relationship with orthorhombic  $\text{Ag}_2\text{Se}$ . The  $a$ - and  $c$ -axis of wurtzite  $\text{CdSe}$  have lattice constants quite similar to the  $c$ - and  $a$ -axis of orthorhombic  $\text{Ag}_2\text{Se}$ , with which the transformation from  $\text{Ag}_2\text{Se}$  to  $\text{CdSe}$  may proceed without substantial rearrangement of the  $\text{Se}^{2-}$  sublattice [23]. As a consequence of this topotactic superimposition, wurtzite  $\text{CdSe}$  which preserved the NR morphology and single crystallinity of the reactant  $\text{Ag}_2\text{Se}$  formed. Such topotactic feature was however less involved in the growth of pure  $\text{ZnSe}$  NRs since wurtzite  $\text{ZnSe}$  did not show topotactic relationship with orthorhombic  $\text{Ag}_2\text{Se}$ . It has been pointed out that the degree of volume change in cation exchange reaction is another important factor directing the morphology and crystallinity of the products [42,43]. The fractional volume change during the

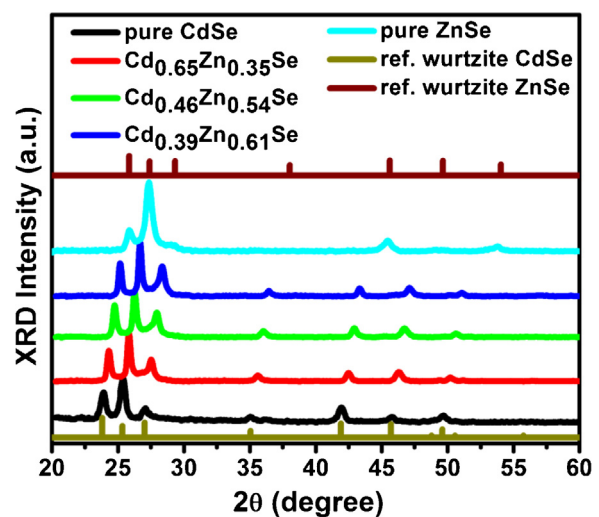


**Fig. 3.** XRD patterns for pure  $\text{CdSe}$ , pure  $\text{ZnSe}$ , and the three individual  $\text{Cd}_{1-x}\text{Zn}_x\text{Se}$  NRs. The patterns of reference wurtzite  $\text{CdSe}$  (JCPDS 08-0459) and wurtzite  $\text{ZnSe}$  (JCPDS 89-2940) were also included for comparison.

transformation from one structure into another can be computed by calculating the volume difference in their unit cells [43], which was estimated to be 0.084 for the conversion of orthorhombic  $\text{Ag}_2\text{Se}$  to wurtzite  $\text{ZnSe}$ . This extremely small volume change may greatly ease the stress accumulation during the transformation, which avoids the structural deformation associated with stress release

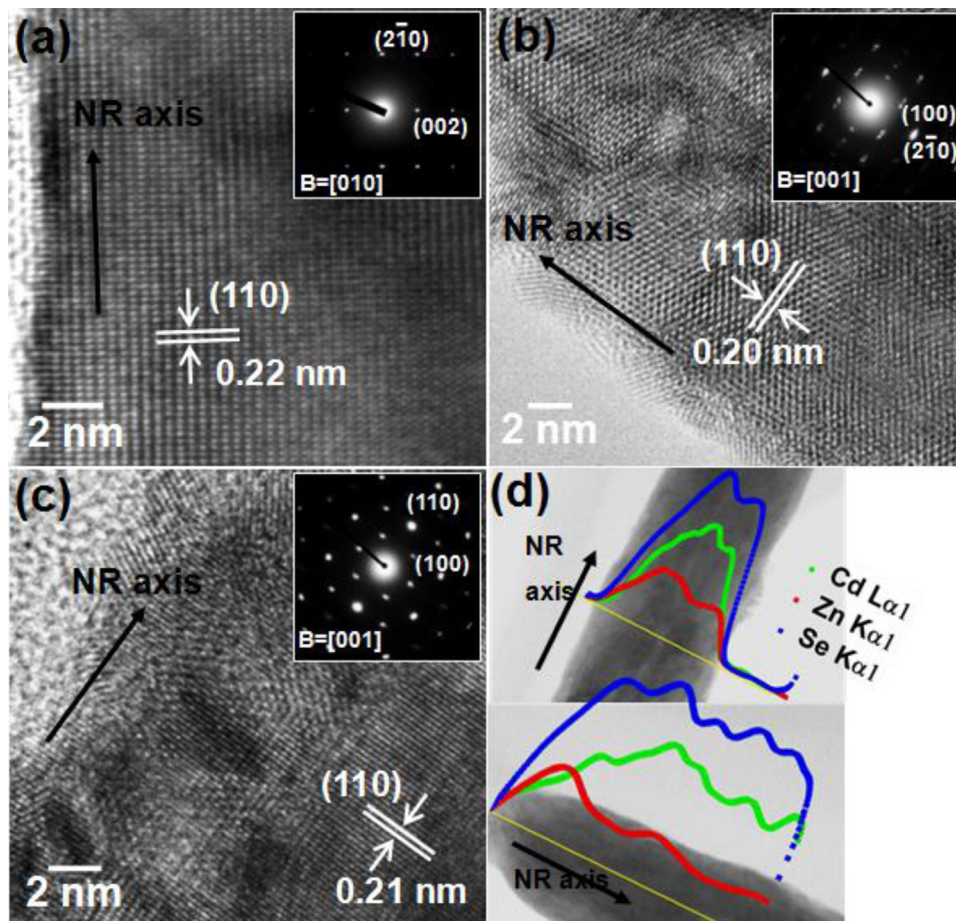


**Fig. 4.** HRTEM images of (a) pure  $\text{CdSe}$ , (b) pure  $\text{ZnSe}$ , and (c)  $\text{Cd}_{0.65}\text{Zn}_{0.35}\text{Se}$  NRs. Insets show the corresponding SAED patterns. (d) TEM-EDS analysis taken on  $\text{Cd}_{0.65}\text{Zn}_{0.35}\text{Se}$  NRs.

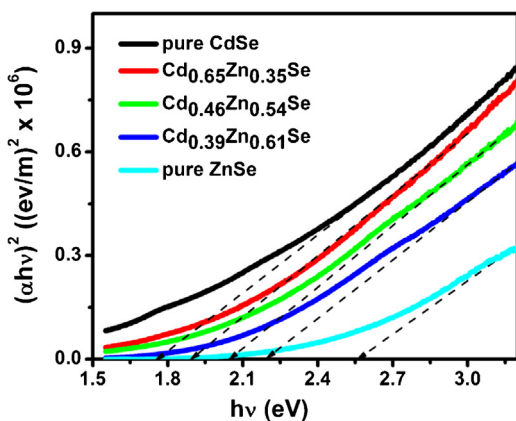
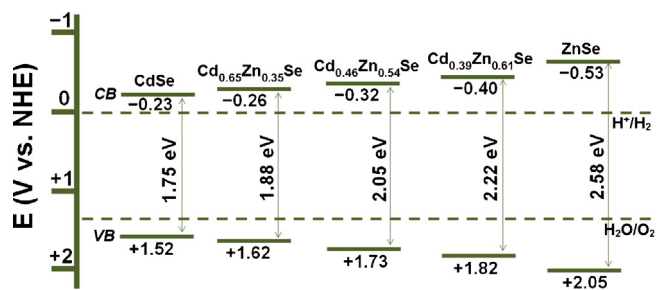


**Fig. 5.**  $(\alpha h\nu)^2$  vs.  $h\nu$  plots for pure CdSe, pure ZnSe and the three individual  $\text{Cd}_{1-x}\text{Zn}_x\text{Se}$  NRs. The band edge position was determined and highlighted with a dashed arrow.

to procure morphological and crystallinity preservation for ZnSe. As to the composite NRs, the pattern, which shifted toward higher  $2\theta$  region with increasing Zn content, was located between those of wurtzite CdSe and wurtzite ZnSe. The dependence of the diffraction peak positions for composite NRs on the corresponding composition was in accordance with Vegard's law [44], further verifying their ternary alloyed structure of  $\text{Cd}_{1-x}\text{Zn}_x\text{Se}$ . It should be noted that no diffraction peaks attributable to  $\text{Ag}_2\text{Se}$  or other impurities could be found in the composite NRs, demonstrating the advantage of the current cation exchange process in preparation of multinary alloyed nanocrystals. Furthermore, the Zn/Cd ratio in the composite NRs was found to be lower than the molar ratio of the precursors added. This may be due to the relatively lower reactivity of the  $\text{Zn}^{2+}$  in the cation exchange reaction with respect to the  $\text{Cd}^{2+}$ , as evidenced by the longer time required for the transformation into ZnSe to complete.

Fig. 4 further shows the detailed crystallographic structure for the three types of NRs derived from  $\text{Ag}_2\text{Se}$ . The dot patterns of the inserted selected area electron diffraction (SAED) images manifest the single-crystallinity for these NRs products. An interlayer spacing of 0.22, 0.20, and 0.21 nm was observed for pure CdSe, pure ZnSe, and  $\text{Cd}_{0.65}\text{Zn}_{0.35}\text{Se}$  NRs, respectively, in agreement with the  $d$  spacing of their (110) lattice planes as determined from the corresponding XRD analysis. Besides, the axis of the NRs was found to be parallel to the [110] direction, implying that these NRs were all grown along the [110] direction. It is worthy of note that no significant diffraction contrast, which would suggest the existence of composition inhomogeneity, was found in each individual  $\text{Cd}_{1-x}\text{Zn}_x\text{Se}$  NR. In Fig. 4(d), the TEM-EDS analysis taken on  $\text{Cd}_{0.65}\text{Zn}_{0.35}\text{Se}$  NRs shows considerably uniform elemental composition along both the radial and axial directions, which reflects a homogeneous distribution of Cd and Zn within the solid matrix of the present  $\text{Cd}_{1-x}\text{Zn}_x\text{Se}$  NRs. This compositional integrity is important to the realization of rainbow photocatalysts because full light harvesting of visible spectrum relies on the synergy of NRs with gradient compositions which are explicit.

As documented in many literature reports [4–6], careful control of the Zn/Cd ratio renders  $\text{Cd}_{1-x}\text{Zn}_x\text{Se}$  effective modulation of absorption band edge, which is imperative for the achievement of full visible photon harvesting. Fig. 5 displays the absorption spectra for the three types of NRs derived from  $\text{Ag}_2\text{Se}$ . The band edge of the samples was determined by performing linear extrapolation of the  $(\alpha h\nu)^2$  vs.  $h\nu$  plot from the absorption shoulder. For pure CdSe and pure ZnSe NRs, the absorption edge was recorded at 1.75 and 2.58 eV, respectively, conforming to their bulk values. As to the ternary  $\text{Cd}_{1-x}\text{Zn}_x\text{Se}$  NRs, the band edge value changed



**Scheme 1.** Calculated band structure of pure CdSe,  $\text{Cd}_{0.65}\text{Zn}_{0.35}\text{Se}$ ,  $\text{Cd}_{0.46}\text{Zn}_{0.54}\text{Se}$ ,  $\text{Cd}_{0.39}\text{Zn}_{0.61}\text{Se}$ , and pure ZnSe NRs. CB and VB represented the conduction and valence band position respectively. Inset dashed lines showed the energy levels of water reduction and oxidation.

from 1.88, to 2.05, and then to 2.22 eV as the Zn content varied from 0.35, to 0.54, and then to 0.61. This blue-shift of band edge with increasing Zn content was attributed to the alloying of lower bandgap material of CdSe with higher bandgap material of ZnSe, quantitatively consistent with the prediction from the optical bowing function established for bulk  $\text{Cd}_{1-x}\text{Zn}_x\text{Se}$  [6,45]. In addition to the shift of bandgap energy, the band structure of  $\text{Cd}_{1-x}\text{Zn}_x\text{Se}$  NRs also revealed a graded variation with the increase of Zn content. The conduction band potential ( $E_{CB}$ ) of  $\text{Cd}_{1-x}\text{Zn}_x\text{Se}$  can be calculated by the empirical equation:  $E_{CB} = X - E^e - 0.5E_g$  [14,46].  $X$  is the geometric mean of electronegativity of the constituent elements, which was estimated to be 5.14, 5.18, 5.20, 5.21 and 5.26 for pure CdSe,  $\text{Cd}_{0.65}\text{Zn}_{0.35}\text{Se}$ ,  $\text{Cd}_{0.46}\text{Zn}_{0.54}\text{Se}$ ,  $\text{Cd}_{0.39}\text{Zn}_{0.61}\text{Se}$  and pure ZnSe NRs, respectively.  $E^e$  is the energy of free electrons on the hydrogen scale (4.5 eV) and  $E_g$  represents the bandgap of the sample. The calculated conduction band potentials of pure CdSe and pure ZnSe were respectively -0.23 and -0.53 V vs. NHE, quite approximate to the values reported in the literature [35,47]. According to the calculation results, the schematic band structure of the samples was determined and depicted in Scheme 1. It can be found that as the bandgap of  $\text{Cd}_{1-x}\text{Zn}_x\text{Se}$  NRs expanded with increasing Zn content, the energy level of conduction band and valence band respectively shifted toward higher and lower potentials. Notably, the conduction and valence band potentials straddled the reduction and oxidation potentials of water, suggesting that the present  $\text{Cd}_{1-x}\text{Zn}_x\text{Se}$  NRs may efficiently catalyze water splitting under light illumination.

The spectral transition for  $\text{Cd}_{1-x}\text{Zn}_x\text{Se}$  NRs with increasing Zn content further inspires us to explore the realization of rainbow photocatalysts by assembling these NRs with different compositions. As sunlight enters the NRs assembly, Zn-rich NRs may absorb the portion of the light with shorter wavelength, while the light with longer wavelength is mainly absorbed by Cd-rich NRs. By creating such a composition-gradient configuration from the assembly of  $\text{Cd}_{1-x}\text{Zn}_x\text{Se}$  NRs, it is possible to attain effective capture of solar spectrum and therefore improve the overall photoconversion efficiency. In order to elucidate the above proposition, we employed the NRs assembly as the photoanode for photoelectrochemical water splitting. Note that the NRs assembly was prepared by mixing equal weights of pure CdSe, pure ZnSe, and the three  $\text{Cd}_{1-x}\text{Zn}_x\text{Se}$  NRs, giving rise to a composition-gradient configuration that may enable full visible photon harvesting. Fig. 6a shows a set of linear sweep voltammograms of the three types of NRs and the NRs assembly recorded in 0.1 M  $\text{Na}_2\text{S}$  electrolyte under white light illumination. The anodic dark current emerging beyond 0.1 V vs.  $\text{Ag}/\text{AgCl}$  could be attributed to the oxidation of PVP molecules adsorbed on the NR surface [48]. Upon light irradiation, all the NR electrodes displayed pronounced photoresponse at the potential range from -0.4 to 0.3 V vs.  $\text{Ag}/\text{AgCl}$ , indicating notable photoactivity for the present NRs within a photoelectrochemical cell.

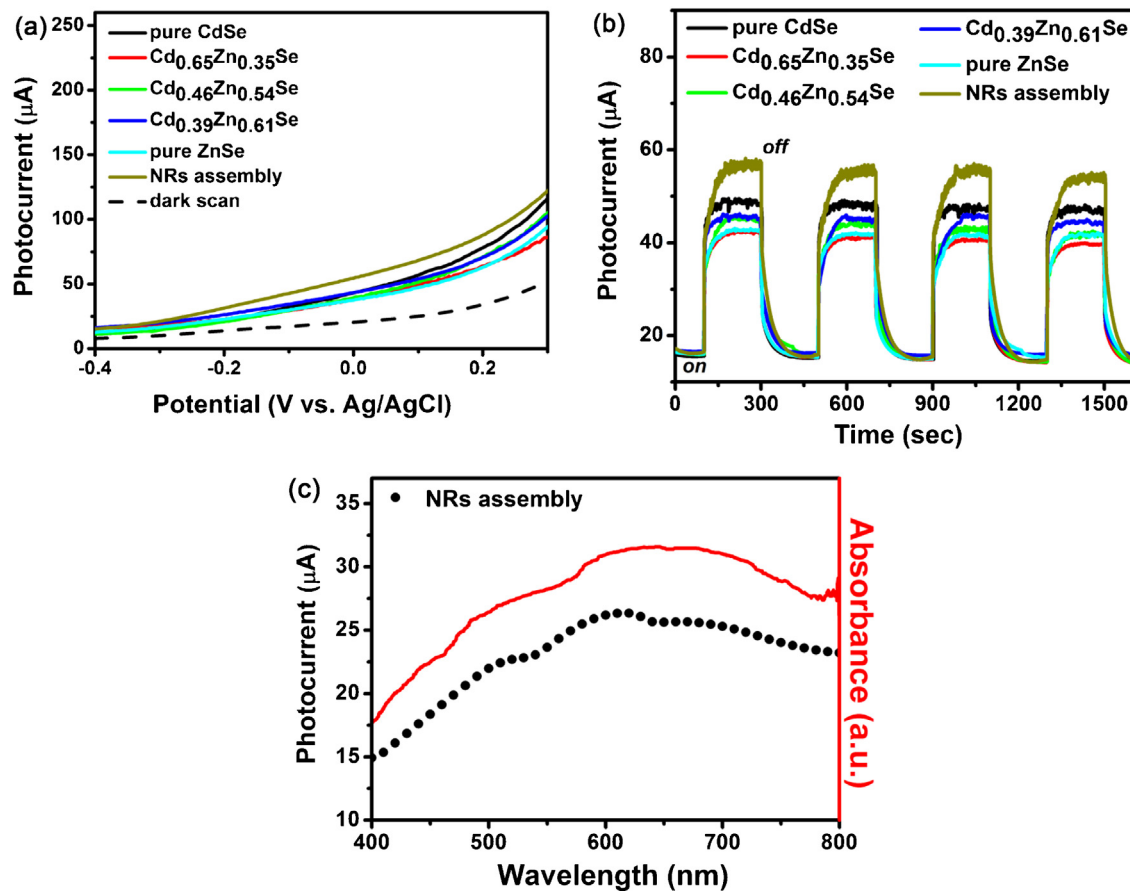


**Fig. 6.** (a) Linear sweep voltammograms of different NRs electrodes recorded in the dark and under white light illumination. (b) Chronoamperometric  $I-t$  curves collected at 0 V vs. Ag/AgCl under white light illumination. (c) Photocurrent action spectrum of NRs assembly collected at 0 V vs. Ag/AgCl in the wavelength range from 400 to 800 nm. The corresponding absorption spectrum was included for comparison.

**Fig. 6b** depicts the corresponding chronoamperometric  $I-t$  curves recorded at 0 V vs. Ag/AgCl under chopped light illumination. All the electrodes were prompt in generating photocurrents with a reproducible response to the on/off cycles of light illumination, suggesting the effective carrier transfer and successful electron collection for the samples during the water splitting process. Significantly, the NRs assembly exhibited considerably higher photocurrents than its individual constituent NRs. This outcome confirms the positive role of composition-gradient configuration for the NRs assembly in enhancing the overall photon harvesting and thus boosting the resultant carrier collection. To further validate the above argument, we measured the photocurrent values at different illumination wavelengths and compared the results with the absorption spectrum. As shown in **Fig. 6c**, the photocurrent action spectrum of the NRs assembly was well-matched with the corresponding absorption spectrum which showed light absorption spanning from 400 to 800 nm. This result signifies that the broadband light absorption feature of the NRs assembly, as a result of the composition-gradient configuration, was responsible for the remarkable photoactivity demonstrated in the photoelectrochemical cell.

To assess the potential as rainbow photocatalysts for the NRs assembly, we performed a series of photocatalysis experiments by using MB as the test pollutant. MB is a cationic dye that can be decomposed by accepting photoexcited electrons following the irradiation on semiconductor photocatalysts [49,50]. The decomposition of MB under light illumination can thus be utilized to evaluate the photoconversion efficiency of the sample. Six kinds of photocatalysts including pure CdSe NRs, pure ZnSe NRs, the three individual  $\text{Cd}_{1-x}\text{Zn}_x\text{Se}$  NRs, and the NRs assembly were used for MB

photodegradation under the same experimental conditions. **Fig. 7a** compares the MB photodegradation results of different samples, from which several points can be observed. First, experiment in the absence of photocatalyst showed a slight degradation of MB, indicating a minor self-photolysis of MB molecules under white light illumination. Second, the photocatalytic efficiency for pure CdSe, pure ZnSe, and the three  $\text{Cd}_{1-x}\text{Zn}_x\text{Se}$  NRs was roughly comparable and merely adequate, with less than 50% of MB being degraded after 180 min of irradiation. Because of the relatively narrow light absorption range, fairly mediocre capture of incident white light was expected for pure CdSe, pure ZnSe and the three  $\text{Cd}_{1-x}\text{Zn}_x\text{Se}$  NRs, which impedes the light harvesting efficiency to cause barely satisfactory photocatalytic performance. It should be mentioned that even though pure CdSe can absorb photons with energy exceeding the bandgap, most of the high-energy photons were converted into heat due to the excitonic relaxation, which results in an essentially depressed photoconversion efficiency and thus the ordinary photocatalytic performance as observed. Third, as compared to the individual constituent NRs, the NRs assembly exhibited superior photocatalytic performance under white light illumination. This superiority emanates from the composition-gradient configuration that significantly improves the light harvesting efficiency by absorbing almost the whole visible spectrum of the incident white light. As a consequence of the full visible photon harvesting, the NRs assembly converted a wide array of photons to exhibit remarkable photocatalytic performance. It is important to state that all the NRs samples showed nearly identical MB adsorption capability since they had comparable surface area of about  $13.4 \text{ m}^2 \text{ g}^{-1}$ . This result signifies that the superior photocatalytic performance of the NRs

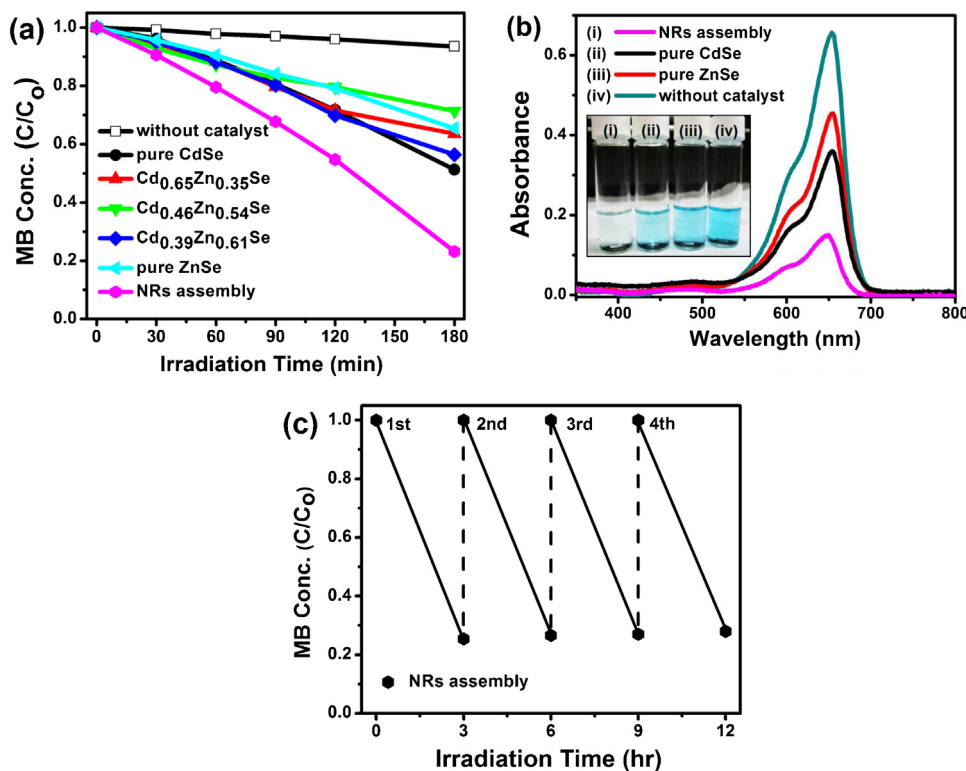


**Fig. 7.** (a) C/Co vs. irradiation time plots for MB photodegradation without any catalyst and in the presence of six relevant samples. (b) Absorption spectra of MB solutions after exposure of 3 h of daytime sunlight without any catalyst and in the presence of pure CdSe NRs, pure ZnSe NRs, or the NRs assembly. Inset shows the corresponding solution color. (c) Recycling test on the NRs assembly for MB photodegradation.

assembly is mainly related to the composition-gradient configuration rather than the structural effect associated with surface area or dye adsorption. It is also important to note that the direct comparison of photocatalytic activity of the NRs assembly with the samples reported in literature is difficult because the experimental setups (e.g. the photoreactor configuration and the irradiation intensity) are essentially different. As a final note, it might be argued that MB sensitization could contribute to the photocatalysis of the samples. Because the lowest-unoccupied molecular orbital (LUMO) potential of MB (+0.05 V vs. NHE) [51] is lower than the conduction band potentials of the present  $\text{Cd}_{1-x}\text{Zn}_x\text{Se}$  NRs (Scheme 1), the electron transfer from the photoexcited MB to the NRs was considered relatively insignificant. The contribution from MB sensitization can thus be excluded as interpreting the photocatalysis results of Fig. 7a.

To further explore the applicability of the NRs assembly in the context of practical solar fuel production, its photocatalytic performance under natural sunlight was evaluated. In this demonstration, three representative samples, pure CdSe, pure ZnSe NRs, and the NRs assembly, were tested and compared. As illustrated in Fig. 7b, after exposure to 3 h of daytime sunlight, nearly 80% of MB was degraded by using NRs assembly, accompanied with an obvious decoloration of the resultant solution. In contrast, pure CdSe and pure ZnSe NRs only degraded 45 and 30% of MB respectively under the same experimental conditions. This activity difference, which is in agreement with the result of Fig. 7a, was due to the difference in light harvesting efficiency between the NRs assembly and the individual constituent NRs. Most importantly, this outcome shows that the assembly of  $\text{Cd}_{1-x}\text{Zn}_x\text{Se}$  NRs with different compositions can be used as practical rainbow photocatalysts for efficient solar fuel production. Furthermore, the recycling test was performed to evaluate the reusability and stability of the NRs assembly. As shown in Fig. 7c, no appreciable decay of photocatalytic activity was found for the NRs assembly after it was repeatedly used and recycled in

MB photodegradation for four times. Besides, SEM examination and EDS analysis showed preserved morphology and composition for the NRs assembly after the recycling test. These results manifest that the present NRs assembly exhibited substantially high stability during their use as photocatalyst. The high stability of the NRs assembly possibly derived from the remaining carbonyl groups of PVP molecules at the NR surfaces, which might mediate the hole transfer to suppress the photocorrosion process [52–54].

#### 4. Conclusions

In conclusion,  $\text{Cd}_{1-x}\text{Zn}_x\text{Se}$  NRs of varying compositions ( $x=0, 0.35, 0.54, 0.61, 1$ ) have been prepared and assembled to demonstrate the realization of rainbow photocatalysts. As compared to the individual constituent NRs, the NRs assembly exhibited higher photocurrents of water splitting as well as superior photocatalytic performance under white light illumination, attributable to the broadband light absorption feature that enables full visible photon harvesting. The current study has successfully carried out the novel concept of rainbow photocatalysts that hold great promise for efficient solar fuel production. Further optimizations of the configuration of the NRs assembly, for example, by constructing a sequentially-layered architecture [10,55] which possesses orderly compositional gradient, may allow maximum photon harvesting to boost the overall photoconversion efficiency.

#### Acknowledgment

This work was financially supported by the National Science Council of Republic of China (Taiwan) under grants NSC-102-2113-M-009-005-MY2 and NSC-102-3113-P-009-002.

## References

- [1] Y. Akdoğan, C. Üzüm, Ö. Dag, N. Coombs, J. Mater. Chem. 16 (2006) 2048–2055.
- [2] M.R. Kim, S.Y. Park, D.J. Jang, J. Phys. Chem. C 114 (2010) 6452–6457.
- [3] S. Sadhu, A. Patra, J. Phys. Chem. C 116 (2012) 15167–15173.
- [4] X. Zhong, M. Han, Z. Dong, T.J. White, W. Knoll, J. Am. Chem. Soc. 125 (2003) 8589–8594.
- [5] X. Zhong, Y. Feng, Y. Zhang, Z. Gu, L. Zou, Nanotechnology 18 (2007) 385606.
- [6] M. Protière, P. Reiss, Small 3 (2007) 399–403.
- [7] E. Jang, S. Jun, L. Pu, Chem. Commun. (2003) 2964–2965.
- [8] A. Pan, R. Liu, M. Sun, C. Ning, ACS Nano 4 (2010) 671–680.
- [9] L.Y. Chen, P.A. Yang, C.H. Tseng, B.J. Hwang, C.H. Chen, App. Phys. Lett. 100 (2012) 163113.
- [10] P.K. Santra, P.V. Kamat, J. Am. Chem. Soc. 135 (2013) 877–885.
- [11] M. Husain, B.P. Singh, S. Kumar, T.P. Sharma, P.J. Sebastian, Sol. Energy Mater. Sol. Cells 76 (2003) 399–415.
- [12] N.J.S. Kissinger, G.G. Kumar, K. Perumal, J. Suthagar, Chin. Phys. Lett. 27 (2010) 057102.
- [13] G. Kartopu, A.J. Clayton, W.S.M. Brooks, S.D. Hodgson, V. Barrioz, A. Maertens, D.A. Lamb, S.J.C. Irvine, Prog. Photovoltaic Res. (Appl. 22, 2014, 18–23.).
- [14] C. Xing, Y. Zhang, W. Yan, L. Guo, Int. J. Hydrogen Energ. 31 (2006) 2018–2024.
- [15] K. Zhang, D. Jing, C. Xing, L. Guo, Int. J. Hydrogen Energ. 32 (2007) 4685–4691.
- [16] M. Liu, L. Wang, G. Lu, X. Yao, L. Guo, Energy Environ. Sci. 4 (2011) 1372–1378.
- [17] X. Wu, Y. Yu, Y. Liu, Y. Xu, C. Liu, B. Zhang, Angew. Chem. Int. Ed. 51 (2012) 3211–3215.
- [18] K.R. Murali, P. Thirumoorthy, Chalcogenide Lett. 8 (2009) 377–384.
- [19] D. Soundararajan, J.K. Yoon, J.S. Kwon, Y.I. Kim, S.H. Kim, J.H. Park, Y.J. Kim, D.-Y. Park, B.C. Kim, G.G. Wallace, J.M. Ko, Bull. Korean Chem. Soc. 31 (2010) 2185–2189.
- [20] C.I. Wang, Z. Yang, A.P. Periasamy, H.T. Chang, J. Mater. 2013 (2013) 703985.
- [21] A. Fujishima, T.N. Rao, D.A. Tryk, J. Photochem. Photobiol. C: Photochem. Rev. 1 (2000) 1–21.
- [22] W.A. Tisdale, K.J. Williams, B.A. Timp, D.J. Norris, E.S. Aydil, X.Y. Zhu, Science 328 (2010) 1543–1547.
- [23] U. Jeong, P.H.C. Camargo, Y.H. Lee, Y. Xia, J. Matter. Chem. 16 (2006) 3893–3897.
- [24] G.D. Moon, S. Ko, Y. Min, J. Zeng, Y. Xia, U. Jeong, Nano Today 6 (2011) 186–203.
- [25] D.H. Son, S.M. Hughes, Y. Yin, A.P. Alivisatos, Sciences 306 (2004) 1009–1012.
- [26] A.M. Smith, S. Nie, J. Am. Chem. Soc. 133 (2011) 24–26.
- [27] L.D. Trizio, M. Prato, A. Genovese, A. Casu, M. Povia, R. Simonutti, M.J.P. Alcocer, C. D'Andrea, F. Tassone, L. Manna, Chem. Mater. 24 (2012) 2400–2406.
- [28] E. Dilena, D. Dorfs, C. George, K. Miszta, M. Povia, A. Genovese, A. Casu, M. Prato, L. Manna, J. Mater. Chem. 22 (2012) 13023–13031.
- [29] A.K. Samal, T. Pradeep, J. Phys. Chem. C 114 (2010) 5871–5878.
- [30] J. Zhang, S. Liu, J. Yu, M. Jaroniec, J. Mater. Chem. 21 (2011) 14655–14662.
- [31] P.H.C. Camargo, Y.H. Lee, U. Jeong, Z. Zou, Y. Xia, Langmuir 23 (2007) 2985–2992.
- [32] S. Panigrahi, D. Basak, RSC Adv. 2 (2012) 11963–11968.
- [33] B. Mukherjee, A. Peterson, V. Subramanian, Chem. Commun. 48 (2012) 2415–2417.
- [34] M. Casavola, M.A. van Huis, S. Bals, K. Lambert, Z. Hens, D. Vanmaekelbergh, Chem. Mater. 24 (2012) 294–302.
- [35] M.-Y. Chen, Y.-J. Hsu, Nanoscale 5 (2013) 363–368.
- [36] R.D. Robinson, B. Sadtler, D.O. Demchenko, C.K. Erdonmez, L.W. Wang, A.P. Alivisatos, Science 317 (2007) 355–358.
- [37] B. Sadtler, D.O. Demchenko, H. Zheng, S.M. Hughes, M.G. Merkle, U. Dahmen, L.W. Wang, A.P. Alivisatos, J. Am. Chem. Soc. 131 (2009) 5285–5293.
- [38] J.M. Luther, H. Zheng, B. Sadtler, A.P. Alivisatos, J. Am. Chem. Soc. 131 (2009) 16851–16857.
- [39] A.K. Samal, T. Pradeep, Nanoscale 3 (2011) 4840–4847.
- [40] A. Som, T. Pradeep, Nanoscale 4 (2012) 4537–4543.
- [41] Y.-D. Chiou, Y.-J. Hsu, Appl. Catal. B: Environmental 105 (2011) 211–219.
- [42] S.E. Wark, C.H. Hsia, D.H. Son, J. Am. Chem. Soc. 130 (2008) 9550–9555.
- [43] G.D. Moon, S. Ko, Y. Xia, U. Jeong, ACS Nano 4 (2010) 2307–2319.
- [44] F.C. Liu, T.L. Cheng, C.C. Shen, W.L. Tseng, M.Y. Chiang, Langmuir 24 (2008) 2162–2167.
- [45] S.A. Santangelo, E.A. Hinds, V.A. Vlaskin, P.I. Archer, D.R. Gamelin, J. Am. Chem. Soc. 129 (2007) 3973–3978.
- [46] J. Hou, Z. Wang, C. Yang, W. Zhou, S. Jiao, H. Zhu, J. Phys. Chem. C 117 (2013) 5132–5141.
- [47] C. Burda, T.C. Green, S. Link, M.A. El-Sayed, J. Phys. Chem. B 103 (1999) 1783–1788.
- [48] T. Ohsaka, Y. Abe, T. Yoshida, Bull. Chem. Soc. Jpn. 46 (1973) 1324–1329.
- [49] I.M. Kobasa, G.P. Tarasenko, Theor. Exp. Chem. 38 (2002) 255–258.
- [50] I.M. Kobasa, I.V. Kondrat'eva, Y.I. Gnatyuk, Theor. Exp. Chem. 44 (2008) 42–47.
- [51] J.-S. Shen, T. Yu, J.-W. Xie, Y.-B. Jiang, Phys. Chem. Chem. Phys. 11 (2009) 5062–5069.
- [52] H. Tsunoyama, N. Ichikuni, H. Sakurai, T. Tsukuda, J. Am. Chem. Soc. 131 (2009) 7086–7093.
- [53] W. Lee, H.J. Son, D.-K. Lee, B.S. Kim, H. Kim, K. Kim, M.J. Ko, Synthetic Met. 165 (2013) 60–63.
- [54] N. Soltani, E. Saion, W.M.M. Yunus, M. Navasery, G. Bahmanrokh, M. Erfani, M.R. Zare, E. Gharibshahi, Solar Energ. 97 (2013) 147–154.
- [55] A. Ruland, C. Schulz-Drost, V. Sgobba, D.M. Guldi, Adv. Mater. 23 (2011) 4573–4577.